

## Structure and Dynamics of Apical Membrane Antigen 1 from *Plasmodium falciparum* FVO

San Sui Lim,<sup>†</sup> Wei Yang,<sup>‡</sup> Bankala Krishnarjuna,<sup>†</sup> Komagal Kannan Sivaraman,<sup>‡</sup> Indu R. Chandrashekaran,<sup>†</sup> Itamar Kass,<sup>‡,§</sup> Christopher A. MacRaild,<sup>†</sup> Shane M. Devine,<sup>†</sup> Cael O. Debono,<sup>†</sup> Robin F. Anders,<sup>†,||</sup> Martin J. Scanlon,<sup>†,⊥</sup> Peter J. Scammells,<sup>†</sup> Raymond S. Norton,<sup>\*,†</sup> and Sheena McGowan<sup>\*,‡</sup>

<sup>†</sup>Medicinal Chemistry, Monash Institute of Pharmaceutical Sciences, Monash University, Parkville, Victoria 3052, Australia

<sup>‡</sup>Department of Biochemistry and Molecular Biology, Monash University, Clayton, Victoria 3800, Australia

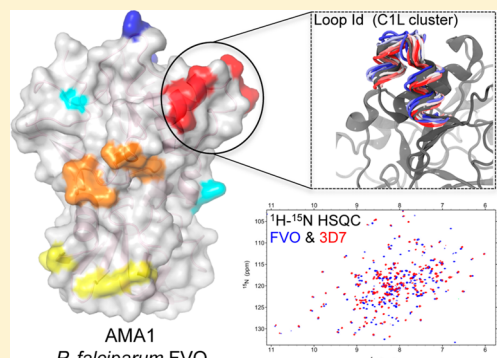
<sup>§</sup>Victorian Life Sciences Computation Initiative Life Sciences Computation Centre, Monash University, Clayton, Victoria 3800, Australia

<sup>||</sup>Department of Biochemistry, La Trobe Institute for Molecular Science, La Trobe University, Bundoora, Victoria 3086, Australia

<sup>⊥</sup>Centre of Excellence for Coherent X-ray Science, Monash University, Parkville, Victoria 3052, Australia

### Supporting Information

**ABSTRACT:** Apical membrane antigen 1 (AMA1) interacts with RON2 to form a protein complex that plays a key role in the invasion of host cells by malaria parasites. Blocking this protein–protein interaction represents a potential route to controlling malaria and related parasitic diseases, but the polymorphic nature of AMA1 has proven to be a major challenge to vaccine-induced antibodies and peptide inhibitors exerting strain-transcending inhibitory effects. Here we present the X-ray crystal structure of AMA1 domains I and II from *Plasmodium falciparum* strain FVO. We compare our new structure to those of AMA1 from *P. falciparum* 3D7 and *Plasmodium vivax*. A combination of normalized *B* factor analysis and computational methods has been used to investigate the flexibility of the domain I loops and how this correlates with their roles in determining the strain specificity of human antibody responses and inhibitory peptides. We also investigated the domain II loop, a key region involved in inhibitor binding, by comparison of multiple AMA1 crystal structures. Collectively, these results provide valuable insights that should contribute to the design of strain-transcending agents targeting *P. falciparum* AMA1.



Malaria is one of the most widespread infections, with more than 40% of the global population at risk of contracting the disease.<sup>1,2</sup> Each year, there are approximately 250 million clinical cases of malaria that result in more than 600000 deaths worldwide.<sup>2</sup> The majority of these deaths are due to *Plasmodium falciparum* infections occurring in young children in sub-Saharan Africa.<sup>2</sup> Although much less likely to cause death, *Plasmodium vivax* infections also contribute to a substantial malaria burden across the globe, with 70–80 million cases occurring annually.<sup>3</sup> Although current artemisinin combination therapies have been highly effective against *Plasmodium* parasites, signs of resistance have already emerged.<sup>4</sup> There is an urgent need to combat this threat using therapeutic agents that act against a broad range of parasite strains, especially those that have become resistant to available therapies.

Apical membrane antigen 1 (AMA1) forms part of the moving junction complex essential for erythrocyte invasion by *Plasmodium* merozoites, and ligands that disrupt AMA1 function inhibit the growth *in vitro* of *P. falciparum* asexual blood stages.<sup>5–9</sup> Further, a conditional knockdown of PfAMA1

severely impaired the parasite's ability to invade red cells,<sup>10</sup> and a complete gene knockout is not viable in *P. falciparum*.<sup>11</sup> AMA1 is a type I integral membrane protein,<sup>12</sup> the extracellular region of which consists of three domains based on the connectivities of its eight intramolecular disulfide bonds: an N-terminal domain I, a central domain II, and a C-terminal domain III.<sup>13,14</sup> Antibodies to AMA1 can block red cell invasion by *P. falciparum* *in vitro* and contribute to the adaptive immune response that partially protects exposed individuals against malaria. AMA1 has been a leading candidate for inclusion in a vaccine against *P. falciparum*,<sup>15</sup> but in a Phase IIb clinical trial in Mali, a 3D7 PfAMA1 vaccine provided protection against only a subset of *P. falciparum* AMA1 genotypes, reflecting the extensive sequence polymorphisms in this antigen.<sup>16</sup> A bivalent 3D7 and FVO PfAMA1 vaccine, also tested in Phase IIb trials, failed to protect because of the poor immunogenicity of the

**Received:** September 25, 2014

**Revised:** October 30, 2014

**Published:** October 31, 2014

alum formulation.<sup>17</sup> Currently, preclinical studies with multi-valent vaccines (four to six AMA1 alleles) show promise, inducing a more broadly cross-reactive antibody response.<sup>18,19</sup>

The two most extensively studied forms of *PfAMA1*, 3D7 and FVO, have 24 amino acid differences, and these polymorphic residues have been grouped into domain I–III clusters based on their spatial proximity on the X-ray crystal structure of 3D7 *PfAMA1*.<sup>20</sup> The domain I cluster is the most important of the three in mediating escape from inhibitory antibodies and was further classified into subclusters C1–C3. Within C1, the region termed C1L is particularly important for immune escape.<sup>18,21</sup> In the preclinical studies of *PfAMA1* vaccines, it was noted that antisera to 3D7 *PfAMA1* were more strain-specific than antisera to FVO *PfAMA1*.

AMA1 has a hydrophobic cleft that is the site of interactions with its protein-binding partner RON2.<sup>9,22</sup> The cleft is surrounded by six loops from domain I (loops Ia–If) and an extended loop from domain II (DII loop).<sup>23</sup> The DII loop appears to contain a strain-transcending epitope as the monoclonal antibody 4G2, which binds to the base of the DII loop, exhibits strain-independent inhibition of *P. falciparum*.<sup>5</sup> We and others have proposed that small molecules targeted to the hydrophobic cleft may interrupt the AMA1–RON2 protein–protein interaction and provide a route to novel therapeutics in the form of protein–protein interaction inhibitors.<sup>24–26</sup> However, polymorphic regions C1 and C3 surrounding one end of the cleft were shown to restrict the cross-reactivity of inhibitory antibodies and peptides such as IgNAR,<sup>7</sup> 1F9,<sup>27,28</sup> and R1.<sup>6,9,29</sup> It has been postulated that sequence variation in the highly polymorphic C1L region (of the C1 subcluster) may result in local secondary structure changes.<sup>15,21</sup> In particular, the presence of a two-turn helix in the Id loop has been questioned for the FVO allele because of the presence of a glycine residue at position 197.<sup>15</sup>

To answer fundamental questions regarding the impact of sequence diversity on AMA1, we have determined the first X-ray crystal structure of *PfAMA1* from FVO. We show through X-ray crystallography, all-atom molecular dynamics, and nuclear magnetic resonance (NMR) spectroscopy that the sequence divergence does not result in structural changes that account for the strain-specific effects documented for inhibitory antibodies and peptides.

## EXPERIMENTAL PROCEDURES

**Protein Expression and Purification.** Domains I and II of the ectodomains of FVO and 3D7 *PfAMA1* (residues 104–438) were produced according to the protocol described by Lim et al.<sup>24</sup> except that the hexa-His tag was removed using TEV protease. The pure His-tagged proteins were dialyzed using membrane tubing (Spectra/Por 3, 3.5 kDa MWCO) against a 100-fold volume of 50 mM Tris (pH 8.0) under constant stirring at 4 °C overnight, and then TEV protease was added to the sample at a 1:30 ratio (w/w) and cleavage allowed to proceed at 4 °C for 48 h with gentle agitation. The mixture was filtered (0.2 μm) and loaded onto a 5 mL CHT I ceramic hydroxyapatite column (Bio-Rad). The cleaved protein was eluted using a linear gradient of 10 to 150 mM phosphate buffers (Na<sub>2</sub>HPO<sub>4</sub> and NaH<sub>2</sub>PO<sub>4</sub>·H<sub>2</sub>O) (pH 7.4) over 15 column volumes. The pooled fractions were concentrated and buffer exchanged into 20 mM Tris (pH 8.0) using an Amicon Ultra-4 centrifugal unit with an Ultracel-10 membrane (Millipore).

**<sup>1</sup>H NMR Spectroscopy and Size-Exclusion Chromatography.** FVO *PfAMA1* purified from hydroxyapatite chromatography was buffer exchanged into 20 mM phosphate buffer (Na<sub>2</sub>HPO<sub>4</sub> and NaH<sub>2</sub>PO<sub>4</sub>·H<sub>2</sub>O) and 50 mM NaCl (pH 7.4) containing 10% <sup>2</sup>H<sub>2</sub>O using a PD-10 desalting column (GE Healthcare). The sample was subsequently concentrated as described above to a final protein concentration of 50 μM. Part of this final product was used for <sup>1</sup>H NMR. A <sup>1</sup>H-detected pulse program incorporating the excitation sculpting scheme for water suppression was employed to characterize FVO *PfAMA1*. A total of 128 scans and 16K data points were acquired at 600 MHz on a Bruker Avance III spectrometer at 35 °C. The data were processed in Topspin 3.2 using an exponential multiplication function with 2 Hz line broadening. The water signal was used to reference the <sup>1</sup>H NMR spectrum. The final product was loaded onto a Superdex 200 10/30 GL column and eluted isocratically with 20 mM phosphate buffer (Na<sub>2</sub>HPO<sub>4</sub> and NaH<sub>2</sub>PO<sub>4</sub>·H<sub>2</sub>O) and 50 mM NaCl (pH 7.4) at a flow rate of 0.5 mL/min.

**<sup>2</sup>H<sub>2</sub>O *Escherichia coli* Adaptation.** Fifty microliters of a competent *E. coli* BL21(DE3) glycerol stock, previously frozen at –80 °C, was thawed on ice for 10 min prior to adding 1 μL of plasmid carrying expression vector pPROEX HTb (Novagen) with FVO or 3D7 *PfAMA1*<sub>[104–438]</sub> sequences. The mixture was left on ice for a further 30 min and then in water at 42 °C for 45 s. One milliliter of Luria broth (LB) was added to each sample, and the culture was incubated at 37 °C while being constantly shaken at 225 rpm. After 45 min, 50 μL of culture was spread over a LB plate containing 50% (v/v) <sup>2</sup>H<sub>2</sub>O and 100 μg/mL ampicillin and then incubated at 37 °C overnight. A single colony of the freshly transformed cells was inoculated into 10 mL of LB medium with 50% (v/v) <sup>2</sup>H<sub>2</sub>O and 100 μg/mL ampicillin. The culture was grown for 24 h at 37 °C while being constantly shaken at 225 rpm. The cell mixture was spread on a culture plate, and subsequently, a single colony of cells was incubated in growth medium as described above, except that the LB plate and medium prepared with 75% (v/v) <sup>2</sup>H<sub>2</sub>O were used instead. The final cell culture containing 75% (v/v) <sup>2</sup>H<sub>2</sub>O was stored at –80 °C with 20% (v/v) glycerol.

**Isotopically Labeled AMA1.** A scrape of the glycerol stock of <sup>2</sup>H<sub>2</sub>O-adapted *E. coli* was inoculated into LB medium with 75% (v/v) <sup>2</sup>H<sub>2</sub>O and 100 μg/mL ampicillin. The culture was incubated overnight at 37 °C while being constantly shaken at 225 rpm. The overnight culture was then centrifuged at 1500g for 15 min. The supernatant was decanted, and the cell pellets were resuspended in 2 volumes of optimized minimal medium<sup>30</sup> prepared with 100% (v/v) <sup>2</sup>H<sub>2</sub>O, 1 g/L <sup>15</sup>NH<sub>4</sub>Cl, and 8 g/L [<sup>13</sup>C]glucose. The cells were allowed to grow for 3 h while being shaken at 37 °C before being induced with 1 mM isopropyl β-D-1-thiogalactopyranoside (IPTG) for 24 h. The protein was then purified as described above.

**<sup>1</sup>H–<sup>15</sup>N HSQC and Three-Dimensional (3D) HNCO Experiments.** <sup>2</sup>H-, <sup>15</sup>N-, and <sup>13</sup>C-labeled 3D7 and FVO *PfAMA1* were dissolved at concentrations of 300 and 75 μM, respectively, in 20 mM phosphate buffer (Na<sub>2</sub>HPO<sub>4</sub> and NaH<sub>2</sub>PO<sub>4</sub>·H<sub>2</sub>O) (pH 7.0) containing 50 mM L-arginine, 50 mM L-glutamic acid, 0.2% (w/v) protease inhibitor cocktail (Roche), 0.01% (w/v) sodium azide, and 10% (v/v) <sup>2</sup>H<sub>2</sub>O. The FVO *PfAMA1* spectrum was acquired on a Bruker Avance III 600 MHz spectrometer at 35 °C. A spectrum of 3D7 *PfAMA1* was acquired on a Bruker Avance III 800 MHz spectrometer at 30 °C. Both the <sup>1</sup>H–<sup>15</sup>N HSQC and 3D HNCO experiments

were conducted using pulse sequences with transverse relaxation-optimized spectroscopy (TROSY) effects.<sup>31,32</sup>  $^1\text{H}$ - $^{15}\text{N}$  HSQC spectra were acquired with 64 scans at 2048 and 256 data points for the  $^1\text{H}$  and  $^{15}\text{N}$  dimensions, respectively. A total of 32 scans was recorded for the 3D HNCO experiments, with 2048, 128, and 128 data points for the  $^1\text{H}$ ,  $^{15}\text{N}$ , and  $^{13}\text{C}$  dimensions, respectively. Both the direct and indirect dimensions of  $^1\text{H}$ - $^{15}\text{N}$  HSQC and 3D HNCO data were processed using a QSINE window with a phase shift of 2. Linear prediction using 32 coefficients was applied to all indirect dimensions.

**R1–FVO PfAMA1 Interactions.** A Biacore T200 biosensor was employed to measure the interaction between recombinant FVO PfAMA1 DI and DII and the R1 peptide (GL Biochem). Surface plasmon resonance (SPR) experiments were conducted essentially as described previously<sup>24</sup> except that dimethyl sulfoxide was not included in the running buffer. Approximately 8000 RU of protein was coupled in a single flow cell (1000 RU = 1 ng of protein/mm<sup>2</sup>). The binding of R1 peptide<sup>6,29</sup> to FVO PfAMA1 was evaluated using a 2-fold serial dilution ranging in concentration from 15.6 to 500  $\mu\text{M}$ .

**Sequence Alignment and Analysis.** All sequence alignments and analyses were performed using the UniProt online tool (<http://www.uniprot.org/>). Accession numbers for AMA1 sequences used in this study are as follows: UniProt entry Q9TY48 for FVO PfAMA1 and UniProt entry Q7KQK5 for 3D7 PfAMA1. The residues defining the AMA1 hydrophobic cleft and polymorphic sites were obtained from published literature.<sup>7,23,33–35</sup>

**Crystallization, X-ray Data Collection, Structure Determination, and Refinement.** Crystallization conditions for FVO PfAMA1 were identified following a robotic broad screen using the IndexHT (Hampton Research) and JCSGPlus (Molecular Dimensions) crystal screens. Optimization of a single initial hit from the Index screen used the hanging drop vapor diffusion method, with a 1:1 (v/v) ratio of protein to mother liquor (well volume of 0.5 mL). Small, stacked crystals appeared after three months in 25% (v/v) polyethylene glycol 3350, 0.1 M HEPES (pH 7.5), and 0.2 M MgCl<sub>2</sub>. A single crystal was separated from the stacked cluster and cryoprotected by the addition of 10% glycerol prior to data collection.

3D7 PfAMA1 crystals were grown in 12–15% (v/v) polyethylene glycol 3350, 0.02 M MES (pH 6.0), and 10 mM MnCl<sub>2</sub> as detailed in ref 23. 3D7 PfAMA1 crystals were dehydrated overnight in a reservoir solution with an increased level [35% (v/v)] of polyethylene glycol 3350 before cryostabilization in 38% (v/v) polyethylene glycol 3350, 0.088 M MES (pH 6.0), and 44 mM MnCl<sub>2</sub> for 6–8 h prior to data collection. For crystals used to test soaking solvents, 5% (v/v) methanol or Milli-Q water was added to the stabilization solution.

Data were collected at 100 K for all crystals using the Australian Synchrotron micro crystallography MX2 beamline 3ID1. Diffraction images were processed using XDS<sup>36</sup> and AIMLESS<sup>37</sup> from the CCP4 suite.<sup>38</sup> Five percent of each data set was flagged for calculation of  $R_{\text{Free}}$ <sup>39</sup> with neither a sigma nor a low-resolution cutoff applied to the data. A summary of data collection statistics is provided in Table S1 of the Supporting Information.

Structure determination proceeded using the Molecular Replacement method and the program PHASER.<sup>40</sup> A search model for FVO PfAMA1 was constructed by removing the

solvent and flexible loops from a crystal structure of 3D7 PfAMA1 [Protein Data Bank (PDB) entry 1Z40]. A single clear peak in both the rotation and translation functions was evident and packed well within the asymmetric unit. Together with the unbiased features in the initial electron density maps, the correctness of the molecular replacement solution was confirmed. All subsequent model building and structural validation for FVO and 3D7 PfAMA1 structures was conducted using Phenix<sup>41,42</sup> and COOT.<sup>43</sup> Solvent molecules were added only if they had acceptable hydrogen bonding geometry contacts of 2.5–3.5 Å with protein atoms or with existing solvent and were in good  $2F_o - F_c$  and  $F_o - F_c$  electron density. Hydrogen bonds (excluding water-mediated bonds) and salt bridges were calculated using PDBePISA.<sup>44</sup> The coordinates and structure factors are available from the Protein Data Bank (entries 4R1A, 4R19, 4R1B, and 4R1C). Raw data and images are available from TARDIS<sup>45</sup> ([www.tardis.edu.au](http://www.tardis.edu.au)).

**B Factor Analysis.** The *B* factors obtained from PDB files cannot be used directly, because the values may be on different scales because of the application of different refinement procedures.<sup>46</sup> To compare the *B* factors from different structures, the values were normalized as described by Parthasarathy et al.<sup>47</sup> The  $\text{Ca}$  *B* factor values were extracted from FVO PfAMA1 (PDB entry 4R1A) and *P. vivax* AMA1 (PDB entry 1W81) as well as the four 3D7 PfAMA1 crystal structures (PDB entries 1Z40, 4R19, 4R1B, and 4R1C), and normalized using the equation  $B_{\text{normalized}} = (\text{Ca } B \text{ factor} - B_{\text{mean}})/\sigma(B)$ , where  $B_{\text{mean}}$  and  $\sigma(B)$  are the mean value and standard deviation, respectively, of the distribution of observed thermal factors. The average values and standard deviations of normalized *B* factors were calculated for  $\alpha$ -helical and  $\beta$ -sheet regions, loops Ia–If, and the DII loop. Average values were not calculated for regions in which more than half of the amino acid sequence was missing in the crystal structures.

**Molecular Dynamics Simulations.** The dynamics of three different AMA1 structures were studied. Atomic coordinates of *P. vivax* AMA1 (PDB entry 1W81, residues 49–383) and 3D7 PfAMA1 (PDB entry 1Z40, residues 104–438) were obtained from the Protein Data Bank. Coordinates for FVO PfAMA1 (residues 104–438) were obtained in this study. Missing atoms and residues were modeled using MOE 2012.10.<sup>48</sup> Each protein was solvated in a water cubic box consisting of TIP3P water molecules<sup>49</sup> with Na<sup>+</sup> ions added to neutralize any charge. The minimum distance from the surface of the protein to any face of the water box was set to 12 Å for each simulation.

All-atom molecular dynamics (MD) simulations were performed using the NAMD 2.9 MD package<sup>50</sup> on the IBM Blue Gene/Q supercomputer of the Victorian Life Sciences Computation Initiative (VLSCI). Proteins were defined by the newly published and tested AMBER force field, FF12SB.<sup>51–53</sup> Equilibration was performed in three stages. First, potential steric clashes in the initial configurations were relieved with 50000 steps of energy minimization. Initial velocities for each system were assigned randomly according to a Maxwell–Boltzmann distribution at 100 K. Each system was then heated to 300 K over 0.1 ns, with the protein harmonically restrained (10 kcal mol<sup>-1</sup> Å<sup>-2</sup>) under the canonical ensemble (NVT) conditions. Following this, each system was simulated for an additional 0.1 ns under the isothermal–isobaric ensemble (NPT) conditions with all heavy protein atoms harmonically restrained (10 kcal mol<sup>-1</sup> Å<sup>-2</sup>). Thereafter, each system was subjected to 250 ns of free simulation.

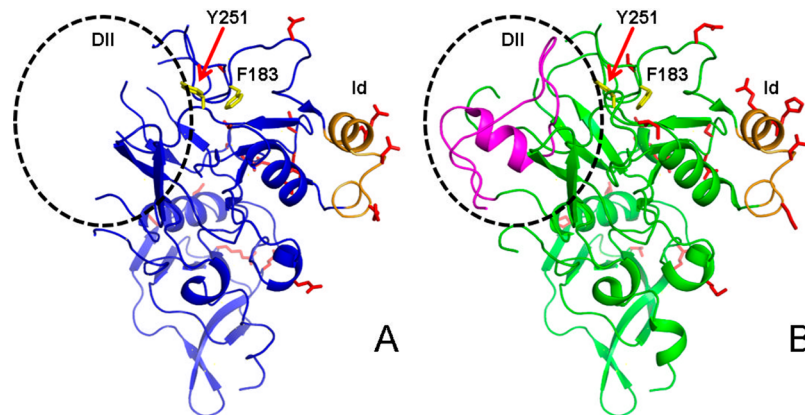


**Figure 1.** X-ray crystal structures of (A) FVO (PDB entry 4R1A) and (B) 3D7 (PDB entry 1Z40) *PfAMA1*. Residues that vary between FVO and 3D7 *PfAMA1* proteins are shown as red sticks. The Id loops are colored orange in both structures. The DII loop is indicated by the dotted circle in both panels, and the structure of the DII loop in 1Z40 is colored magenta (B). Two residues critical for the AMA1–RON2 interaction (Phe183 and Tyr251) are shown as yellow sticks in both structures. The hydrophobic cleft runs across the top of the molecule in this view, from the Id loop at one end to the DII loop at the other.

For all simulations, an integration time of 2 fs was used and the nonbonded cutoff length was set at 1 nm. All simulations were conducted at a constant temperature (300 K) and pressure (1 atm), using a Langevin damping coefficient of 0.5  $\text{fs}^{-1}$ . For each simulation system, periodic boundary conditions (*PBC*) were used together with the particle mesh Ewald (*PME*) method for electrostatics interactions.<sup>54</sup> Electrostatics and VDW nonbonded forces were cut off at 1 nm. For each protein, three trajectories were run in parallel, differing only in the distribution of their initial velocities. System conformations were saved every 10 ps for subsequent analysis.

All the analyses were performed using the GROMACS 4.0.7 simulation software package.<sup>55</sup> Prior to MD analyses, translational and rotational motions were eliminated by superposition of each frame onto the initial conformation. The root-mean-square deviations (rmsds) of the backbone heavy atoms in each system were calculated relative to their corresponding initial minimized structures. Backbone root-mean-square fluctuations (rmsfs) were calculated for the productive phase (50–250 ns) of each simulation. All images were created by VMD version 1.9.1<sup>56</sup> or PyMOL version 1.3r2 (Schrodinger, LLC, 2010, The PyMOL Molecular Graphics System).

**Electrostatic Surface Potential Calculations.** Protein electrostatic potentials were calculated using APBS version 1.3.<sup>57</sup> Atom electrostatic charges were taken from the FF12SB force field. The electrostatic potential was visualized using PyMOL 1.3r2 (Schrodinger, LLC) with positive potential in blue and negative potential in red over the range of  $-3k_bT/e_c$  to  $3k_bT/e_c$ , where  $k_b$  is the Boltzmann constant,  $T$  is the temperature (set to 300 K), and  $e_c$  is the electron charge.

**Effect of Mutations on the Stability of the R1–3D7 *PfAMA1* Complex.** The contributions of specific mutations to the overall thermodynamic stability of the R1–3D7 *PfAMA1* complex structure<sup>9</sup> were estimated *in silico* with FoldX using default settings.<sup>58</sup> The reported Gibbs free energies are the differences between those of wild-type and mutated 3D7 *PfAMA1* in the context of the complex.

## RESULTS

**X-ray Crystal Structure of FVO *PfAMA1*.** To generate protein crystals of FVO *PfAMA1*, a construct of FVO domains I and II (DI + II) equivalent to that of 3D7 *PfAMA1* was

produced.<sup>23</sup> The quality of our recombinant FVO *PfAMA1* protein was assessed using  $^1\text{H}$  NMR spectroscopy and size-exclusion chromatography (Figure S1 of the Supporting Information). Overall, good signal dispersion was observed in the  $^1\text{H}$  NMR spectrum, with methyl proton signals at  $-0.48$  and  $-0.52$  ppm as well as amide proton signals beyond 9 ppm (Figure S1A of the Supporting Information); the spectrum was consistent with a single folded product. During size-exclusion chromatography, FVO *PfAMA1* eluted as a single peak consistent with a monomeric form of the protein (38 kDa) (Figure S1B of the Supporting Information).

The X-ray crystal structure of FVO *PfAMA1* was determined to 2.0 Å with final  $R$  and  $R_{\text{free}}$  values of 19.5 and 25.5%, respectively (Figure 1A and Table S1 of the Supporting Information). FVO *PfAMA1* crystallized with one molecule in the asymmetric unit in space group  $C2_1$ . Seven  $\alpha$ -helical and 16  $\beta$ -sheet regions were identified in the final FVO *PfAMA1* structure. Similar to the 3D7 *PfAMA1* (Figure 1B, PDB entry 1Z40) and *P. vivax* AMA1 structures (PDB entry 1W81), both DI and DII of FVO *PfAMA1* formed PAN folds that consist of a two-turn  $\alpha$ -helix packed against a five-stranded  $\beta$ -sheet. The two PAN folds pack against each other to form the protein core, as seen in the 3D7 *PfAMA1*<sup>23</sup> (PDB entry 1Z40; 0.27 Å rmsd over 219  $\text{C}\alpha$  atoms) and *P. vivax*<sup>59</sup> AMA1 (PDB entry 1Z40; 0.29 Å rmsd over 197  $\text{C}\alpha$  atoms) structures. The DI + II sequences of 3D7 and FVO *PfAMA1* have 21 amino acid residue differences [sharing 94% sequence identity (Figure S2 of the Supporting Information)].

All residue differences found in the C1 (residues 187, 190, 196, 197, 200, 204, 206, and 225) and C2 (residues 242, 243, 282, 283, and 285) clusters can be observed in our FVO *PfAMA1* structure (Figure S2 of the Supporting Information). Structural analysis of regions in the vicinity of the C1L (residues 196, 197, 200, 204, and 206), C2, and DII clusters, as well as residues 167 and 300, did not reveal any significant structural differences between FVO and 3D7 *PfAMA1* DI + II (Figure S3 of the Supporting Information). Structural differences were also not found in regions around residues 187 and 190 within the C1 cluster. Of the regions in the proximity of residue 225, residues 226–232 are disordered in FVO *PfAMA1* but ordered in 3D7 *PfAMA1*. Structural comparisons could not be performed for C3 because residues 175 and 267, which

constitute this cluster, are disordered in both structures. Nine of the 12 residues that define the hydrophobic cleft could be observed in our FVO *PfAMA1* structure (V169, L176, F183, I190, Y202, V208, M224, Y251, and I252);<sup>7</sup> the three remaining hydrophobic residues (M273 from DI and L357 and F367 from DII) are disordered in the FVO *PfAMA1* structure.

The structure of FVO *PfAMA1* showed numerous disordered loops in both domains. In DI, the disordered residues not observed in the density (160–163, 173–176, 226–232, and 258–273) correspond to loops Ib and If and part of the Ie loop (Figure 1A). There are 38 residues missing in DII [351–388 (Figure 1A)], which correspond to most of the loop DII structure found in the 3D7 *PfAMA1* structure (Figure 1B).

#### Flexibility of the Loops in Different Forms of AMA1.

To ascertain whether the sequence polymorphisms might provide a structure-based “escape” route from the host immune response and inhibitor binding, we analyzed the loop flexibility of our FVO *PfAMA1* structure in comparison to those of the published 3D7 *PfAMA1* (PDB entry 1Z40) and *P. vivax* AMA1 (PDB entry 1W81) structures. We compared normalized *B* factors from all  $C\alpha$  atoms from each AMA1. The normalized *B* values were expressed in units of standard deviations about the mean  $C\alpha$  *B* factor for the corresponding structure; therefore, regions that are more rigid in a protein would have low normalized *B* factors, whereas flexible regions would have high normalized *B* values. This analysis showed that loops Ib and If (polymorphic cluster C3) are highly flexible regions in all three structures (Figure 2 and Table S2 of the Supporting Information). Loops Ia, Ic (residues 187 and 190 of the C1 cluster), and Ie (residue 225 of the C1 cluster) are mobile in

FVO *PfAMA1* and *P. vivax* AMA1 but exhibit limited mobility in 3D7 *PfAMA1*. The Id loop (C1L cluster) appears to be more rigid in FVO *PfAMA1* than in 3D7 and *P. vivax* AMA1, but inferring the biological relevance of this result is difficult because of the presence of extensive crystal contacts made by residues within the Id loop of FVO *PfAMA1* (Figure S4 of the Supporting Information; see below).

In an effort to further assess the flexibility of the three AMA1 proteins, we undertook all-atom molecular dynamics simulations. Throughout our MD simulations, all systems were found to be stable following an initial structural rearrangement that took place early in the simulations (30–50 ns). Therefore, all subsequent analyses were conducted for the last 200 ns of each simulation (productive stage). Calculated rmsd values for the productive stage of MD simulations [3D7 *PfAMA1*,  $0.19 \pm 0.04$  nm; FVO *PfAMA1*,  $0.20 \pm 0.03$  nm; and *P. vivax* AMA1,  $0.30 \pm 0.05$  nm (Figure S5 of the Supporting Information)] indicated that all systems were stable and that the *P. vivax* protein was slightly more flexible than the other proteins [particularly in the region of loop Ia (Figure S6 of the Supporting Information)]. The rmsf results (Figure S6 of the Supporting Information) show that the fluctuation patterns of the three proteins were similar, with peak fluctuations occurring in the same loops of each AMA1 structure (loops Ib, Ic, Ie, and If), which is consistent with the *B* factor analysis. The Ie loop appears to be more flexible in FVO *PfAMA1* than in 3D7 *PfAMA1*. This observation may explain why the Ie loop is disordered in the FVO *PfAMA1* crystal structure but not in 3D7 *PfAMA1*. On the basis of the rmsf results, the Id loop is flexible in all three AMA1 structures, which supports our earlier conclusions that the rigidity of the Id loop (Figure 2B) seen in FVO *PfAMA1* was a consequence of crystal contacts.

Crystallization artifacts, such as crystal contacts, can often complicate structural comparisons and implications drawn from static structures. The presence of stabilizing crystal contacts was identified in the original 3D7 *PfAMA1* structure by Bai et al.<sup>23</sup> In the search for suitable crystallization conditions of 3D7 *PfAMA1* for our fragment screening campaign,<sup>24</sup> we noticed that such crystal contacts could be modulated by soaking crystals in different solvents. This allowed us to examine the effect of these contacts on the conformation and/or flexibility of the surface loops in 3D7 *PfAMA1*. We reproduced the original crystal conditions of Bai et al.,<sup>23</sup> determined the 1.8 Å X-ray crystal structure (PDB entry 4R19), and showed that it was identical to the published structure (PDB entry 1Z40; 0.118 Å rmsd over 275  $C\alpha$  atoms). Under these conditions, 3D7 *PfAMA1* crystallized in a  $P3_1$  space group with two molecules per asymmetric unit and showed crystal contacts that potentially stabilize the Ia–If and DII loops surrounding the hydrophobic cleft (Table S3 of the Supporting Information). Subjecting the crystals to 5% methanol (PDB entry 4R1C) or water (PDB entry 4R1B) during their stabilization immediately prior to data collection produced changes in the space group and unit cell dimensions (Table S1 of the Supporting Information), and these two new 3D7 *PfAMA1* structures showed different degrees of flexibility within the Ia, Ic, and Ie loops relative to the published 3D7 *PfAMA1* structure (Table S2 of the Supporting Information). The 3D7 *PfAMA1* structures from the Milli-Q water- and methanol-treated crystals have higher average normalized *B* factors for the Ia, Ic, and Ie loops compared to those of the 1Z40 structure (Figures 3 and 4). The Ie loop of FVO *PfAMA1*, which is disordered, is ordered in all the 3D7 *PfAMA1* structures.

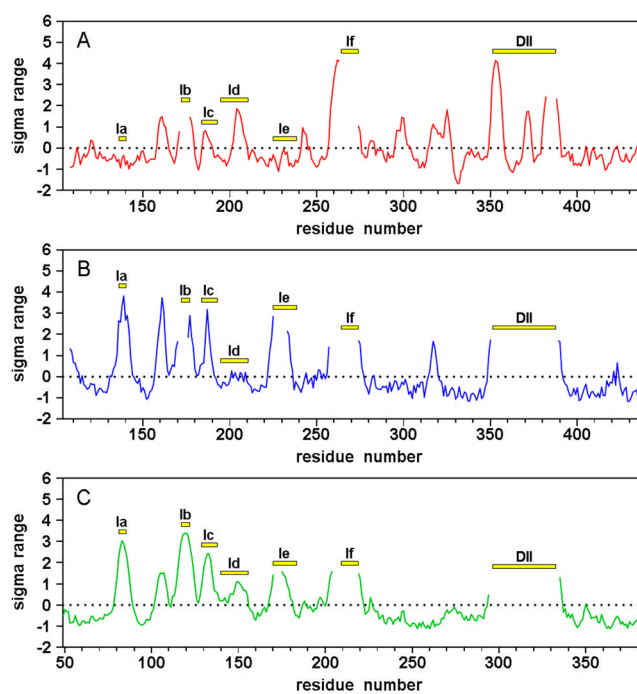


**Figure 2.** Flexibility of Ia–If and DII loops (identified with yellow bars). Normalized  $C\alpha$  *B* factors of (A) 3D7 *PfAMA1* (PDB entry 1Z40), (B) FVO *PfAMA1* (PDB entry 4R1A), and (C) *P. vivax* AMA1 (PDB entry 1W81). Residues 49–383 for the *P. vivax* AMA1 sequence are equivalent to residues 104–438 in the FVO and 3D7 *PfAMA1* sequences.

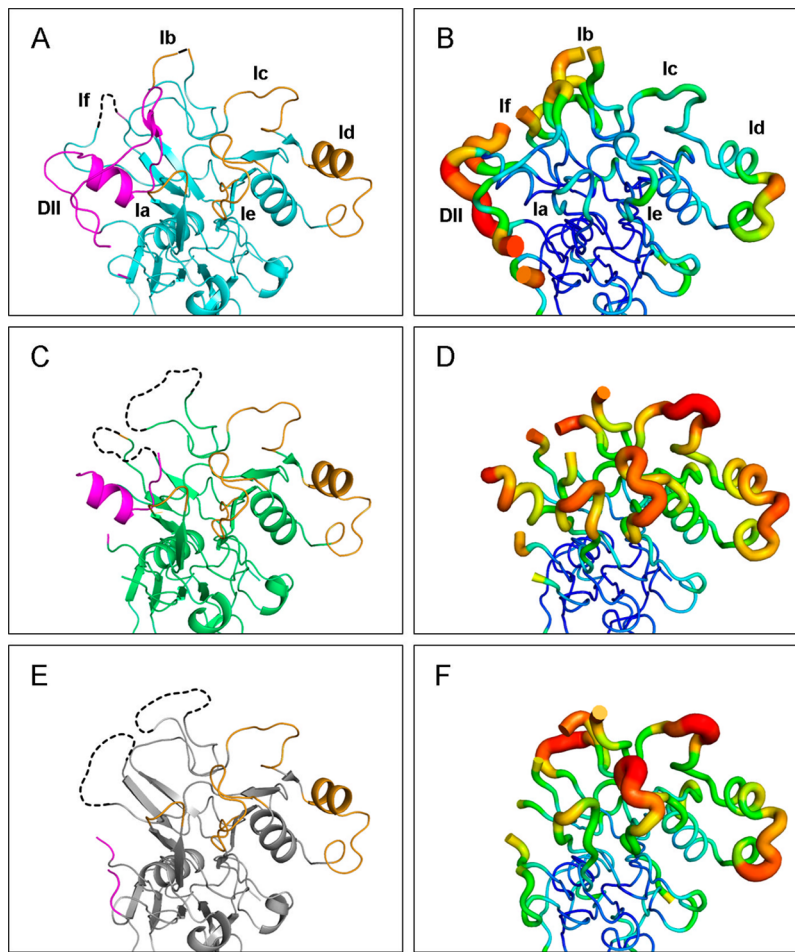


**Figure 3.** Cartoon model (left) and *B* factor putty (right) of the X-ray crystal structures of 3D7 *PfAMA1*: (A and B) 3D7 crystal structure from ref 23, (C and D) 3D7 crystal treated with Milli-Q water (PDB entry 4R1B), and (E and F) 3D7 crystal treated with methanol (PDB entry 4R1C).

However, it is difficult to determine if there is a real difference in the flexibility of the Ie loop as crystal packing is found in all the 3D7 *PfAMA1* structures (Table S3 of the Supporting Information). The Ib and If loops are disordered in both the water- and methanol-treated 3D7 *PfAMA1* crystals, indicating that these regions are highly mobile in the protein (Figures 3 and 4 and Table S2 of the Supporting Information).

**Conformational Flexibility of the DII Loop.** The DII loop in both *P. vivax* AMA1 and our FVO *PfAMA1* (Figure 1A) structure is disordered. This is in contrast to the published 3D7 *PfAMA1* structure in which only five residues are missing from the DII loop (residues 383–387) (Figure 1B). However, there was missing density for DII loop residues 370–387 in our Milli-Q water-treated 3D7 *PfAMA1* structure and residues 351–387 in the methanol-treated 3D7 *PfAMA1* structure, similar to our FVO *PfAMA1* structure (Figures 1B and 3). MD simulations showed that, although the N- and C-termini of the DII loop are highly mobile for FVO *PfAMA1*, 3D7 *PfAMA1*, and *P. vivax* AMA1 (Figure S6 of the Supporting Information), large conformational changes or movements of the  $\alpha$ -helix at the center of the DII loop were not observed in any of these proteins. This implies that, despite its flexibility, the DII loop undergoes slow conformational exchange, beyond the time scale sampled in our MD simulations.

The original 3D7 *PfAMA1* structure (PDB entry 1Z40) provides support for the DII loop being ordered as a consequence of crystal contacts.<sup>23</sup> Our investigation of these

contacts found that there were 9 and 13 residues from neighboring molecules close to ( $<4.0 \text{ \AA}$ ) the DII loop of reference 3D7 *PfAMA1* chains A and E, respectively (Figure S7A of the Supporting Information). In particular, we found that both Glu354 (O $\epsilon$ 1) and His356 (NH) of chain E formed hydrogen bonds with the main and side chains of Ser423 of a symmetry-related molecule (Figure S7A of the Supporting Information). The DII loop of chain A was stabilized by polar interactions between Lys363 (N $\zeta$ ) and Asp317 of a symmetry-related molecule. In our FVO structure, there are no crystal contacts close to the DII loop, possibly allowing the loop to populate different positions within the crystal lattice (Figure S7B of the Supporting Information).

NMR studies of FVO and 3D7 *PfAMA1* were undertaken to further assess their flexibility in solution. Both 2D  $^1\text{H}-^{15}\text{N}$  HSQC and 3D HNCO spectra were acquired. Of the 316 amide backbone NMR resonances expected in both forms of *PfAMA1*, only 261 and 250 peaks were identified in the HSQC spectra of FVO and 3D7 *PfAMA1*, respectively (Figure S8 of the Supporting Information). The discrepancies between the expected and observed resonances are due to regions of the protein that undergo conformational exchange on the intermediate time scale (microseconds to milliseconds).<sup>60</sup> NMR signals from regions with such motion are often broadened beyond detection in multidimensional NMR experiments. In the HNCO spectra, there were fewer resonances in 3D7 *PfAMA1* than in FVO *PfAMA1* [248 and

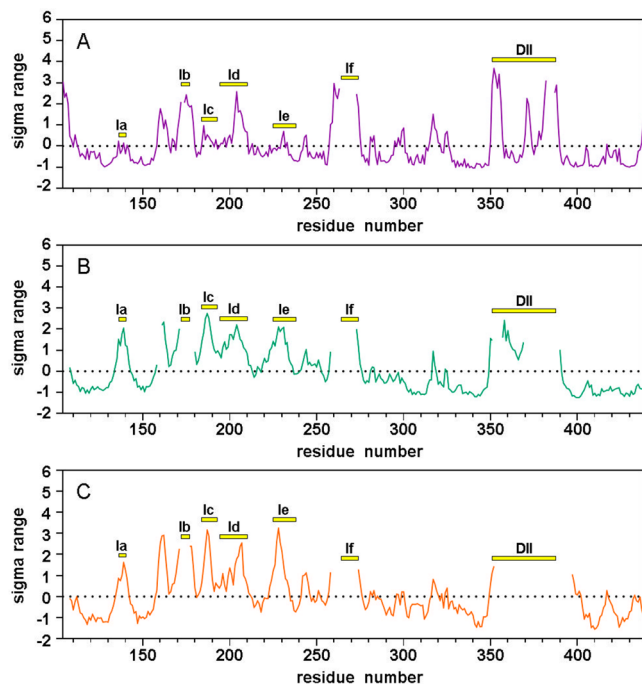


**Figure 4.** Flexibility of Ia–If and DII loops (identified with yellow bars) in 3D7 *PfAMA1*. Normalized  $C\alpha$  B factors of (A) the 3D7 original condition,<sup>23</sup> (B) the 3D7 crystal treated with Milli-Q water, and (C) the 3D7 crystal treated with methanol.

216 peaks in FVO and 3D7 *PfAMA1*, respectively (Figure S9 of the Supporting Information)]. This difference suggests that 3D7 *PfAMA1* has a slightly greater number of backbone resonances that are broadened by intermediate conformational exchange than FVO *PfAMA1*. This is in contrast to what is predicted from comparison of the published 3D7 *PfAMA1*

structure (PDB entry 1Z40), which is highly ordered throughout the molecule, with our crystal structures of both FVO *PfAMA1* and 3D7 *PfAMA1* in different solvents. In summary, these data indicate that in solution both FVO *PfAMA1* and 3D7 *PfAMA1* contain significant regions of disordered structure, some of which are undergoing conformational exchange on an intermediate time scale that produces substantial broadening of NMR resonances.<sup>60</sup>

**Mapping the Strain Variation of the Inhibitory Peptide R1.** The R1 peptide,<sup>6,29</sup> identified by phage display, inhibits red cell invasion by merozoites of 3D7 *P. falciparum* and related strains with a 50% inhibitory concentration ( $IC_{50}$ ) of  $\sim 0.1 \mu M$ . X-ray crystal structures<sup>23,25</sup> show that R1 contacts three polymorphic residues (Tyr175, Met224, and Ile225) in 3D7 *PfAMA1*, with residues at positions 175 and 225 being important determinants of R1 strain specificity. Substitution of these residues as in W2mef (I225E) or HB3 (Y175D and I225N) significantly reduced the peptide's inhibitory effect.<sup>9</sup> FVO *PfAMA1* also has Y175D and I225N substitutions (Figure S2 of the Supporting Information). Accordingly, we found that R1 binds weakly to FVO *PfAMA1*, with an estimated  $K_d$  of  $\geq 500 \mu M$  (Figure S10 of the Supporting Information).

To investigate why R1 binds so weakly to FVO *PfAMA1*, we estimated the effect of mutations on binding of R1 by FVO *PfAMA1*. The crystal structure of the 3D7 *PfAMA1*–R1 complex (PDB entry 3SRJ) was used as a template, and four FVO *PfAMA1* sequence variations found in the R1-binding cleft (Y175D, M190I, D204N, and I225N) were generated by FoldX 3.0<sup>61,62</sup> to mimic an apparent FVO *PfAMA1*–R1 complex-binding structure (Figure 5). Single mutations were also generated to compare the individual effects on the binding energy. Analysis of point mutations shows that the changes at positions 175 and 225 (Y to D and I to N, respectively) had the largest effect on stability, with increases in free energy of 6 and

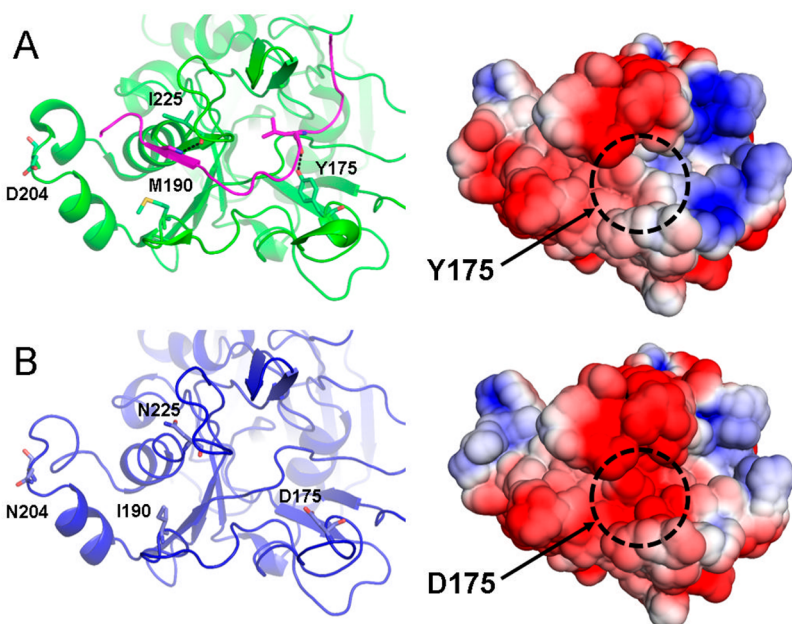


**Figure 5.** Comparison between the R1–3D7 *PfAMA1* complex and free FVO *PfAMA1*. (A) R1–3D7 *PfAMA1* crystal structure (PDB entry 3SRJ). (B) FVO *PfAMA1* model. Electrostatic potentials mapped on the solvent accessible surface for the R1-bound *PfAMA1* structures are shown on the right. Sequence variations between 3D7 and FVO *PfAMA1* are shown as sticks. R1 is shown as a magenta ribbon. Protein surfaces are color-coded according to electrostatic potential gradient, where positively and negatively charged areas are colored blue and red (iso-values from  $3k_b T/e_c$  to  $-3k_b T/e_c$ ), respectively.

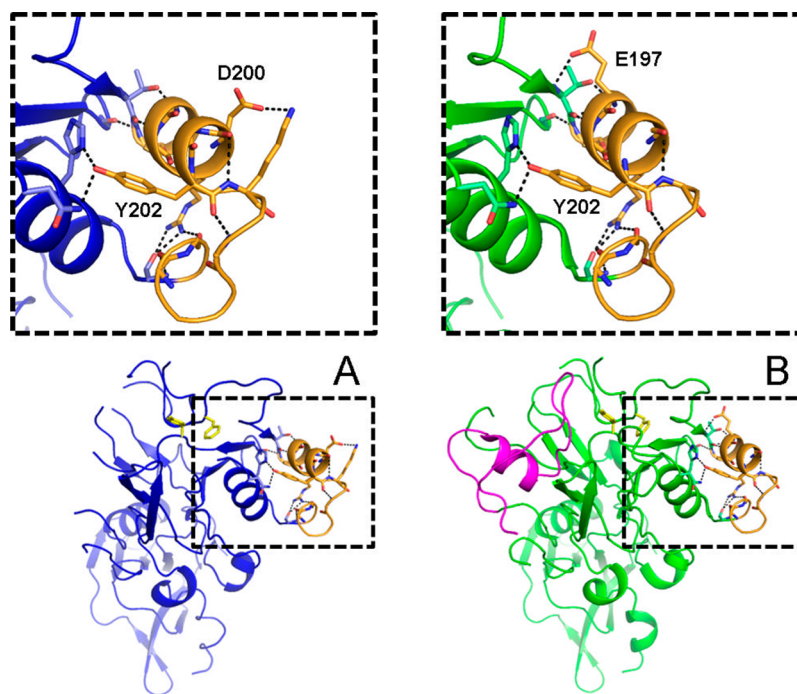


**Figure 6.** Cartoon showing polar interactions that stabilize the Id loop (orange) in (A) FVO (blue) and (B) 3D7 (green) *PfAMA1*. The DII loop is colored magenta. Residues Phe183 and Tyr251 are shown as yellow sticks.

3 kcal/mol, respectively (Table S4 of the Supporting Information). These energy changes are presumably due to the loss of two hydrogen bonds between R1 and AMA1 at these two positions (Figure 5). The M190I change resulted in a small increase in free energy (1 kcal/mol), suggesting that the increase in cleft volume and hydrophobicity resulting from the M190I change has an effect on R1 binding. Distal to the R1 interaction sites, the D204N change has no effect on the complex. Taken together, the four changes were estimated to contribute to a total increase in  $\Delta G$  of 10 kcal/mol and significant changes in the hydrophobic cleft, creating an unfavorable environment for the R1 peptide (Table S4 of the Supporting Information).

## ■ DISCUSSION

AMA1 is implicated in the invasion of host cells by malaria parasites as well as other apicomplexan parasites.<sup>22,25,63,64</sup> Sequence comparison of FVO and 3D7 *PfAMA1* domains I and II identifies 21 amino acid differences that occur exclusively at the polymorphic face of AMA1.<sup>23,33,35</sup> However, despite earlier hypotheses,<sup>15,21</sup> our FVO structure shows that these changes do not influence the overall fold of AMA1. The Ia–If loops that surround most of the hydrophobic cleft in AMA1 all display some level of disorder in the electron density from the FVO *PfAMA1*, 3D7 *PfAMA1*, and *P. vivax* structures. This apparent loop flexibility coupled with the polymorphic residues found in most of these regions provides AMA1 with an effective means of restricting cross-strain inhibitory activities of various ligands such as the R1 peptide and poses a challenge to efforts to design a vaccine or therapeutic agents effective against a broad range of strains and species of *Plasmodium* parasites.

Polymorphic residues within loop Id (C1L cluster) are important in mediating escape against AMA1 antibodies induced by *P. falciparum* infections or in vaccine trials.<sup>23,25,65</sup> Residue 197 appears to be one of the most important residues in AMA1 responsible for immune escape.<sup>65,66</sup> In this study, we

have shown that residue changes, including a Gly at position 197, do not result in structural changes in this region. This includes the two-turn helix within C1L. Residues 196, 204, and 206 are not engaged in any polar interactions and are unlikely to be important in stabilizing the structure of the Id loop (Table S5 of the Supporting Information). The main chain atoms of residues 197 and 200 in both strains form polar interactions with main chain atoms of Thr194 and Lys203, respectively. Substitution of Glu with Gly at position 197 in FVO *PfAMA1* prevents the polar interaction between Thr194 [O] and Glu197 [O $\gamma$ 1] observed in 3D7. The H200D change at position 200 results in an additional side chain electrostatic interaction between Asp200 [O $\delta$ 1] and Lys203 [N $\zeta$ ] in the FVO form of AMA1. The extensive pattern of hydrogen bonds stabilizing the Id loop is largely conserved in both strains (Figure 6 and Table S5 of the Supporting Information). These interactions appear to stabilize the structure and permit radical changes at polymorphic sites in the Id loop without causing significant conformational changes. This implies that the polymorphic nature of this region does not affect the structure of the protein and that immune escape arises largely from changes in properties of individual side chains.

Unlike the published structures of 3D7 *PfAMA1* and one 1F9–3D7 *PfAMA1* complex (PDB entries 1Z40 and 2Q8A, respectively), in which the conserved DII loop is partially ordered, the DII loop of FVO *PfAMA1* is completely disordered. This is similar to the case in another crystal form of the 1F9–3D7 *PfAMA1* complex (PDB entry 2Q8B)<sup>27</sup> and the *P. vivax* AMA1 structure (PDB entry 1W81).<sup>59</sup> The flexibility of the DII loop is linked to a conformational change that allows the protein to interact with its protein-binding partner, RON2 (PDB entry 3ZWZ).<sup>27</sup> By sequence and structural superposition, it appears that the intraprotein contacts involved in stabilizing the local secondary structure of the DII loop are maintained in FVO *PfAMA1*. The differences observed between the crystal structures of the two

forms of AMA1 reflect different individual conformational states captured under the different crystallization conditions rather than an inherently greater level of disorder in the FVO *PfAMA1* DII loop. This view is further supported by our 3D7 *PfAMA1* structures, in which different extents of crystal contacts gave rise to different degrees of order in the DII loop.

In conclusion, our results show that the overall structure, including the flexible nature of the DII loop, is conserved between the FVO and 3D7 forms of AMA1. The interacting interfaces between DI and the DII loop consist of invariant residues across all *P. falciparum* strains. The structural conservation of DI and DII appears likely to be conserved across all allelic forms of AMA1 and hence represents an attractive site for strain-transcending therapeutic interventions. Given that DII loop displacement is associated with formation of the AMA1–RON2 complex, it is conceivable that stabilizing the DII loop in its ordered state would be inhibitory to AMA1 function.<sup>9</sup> Recently, we have undertaken a fragment-based screening campaign against AMA1 to identify chemical scaffolds capable of inhibiting the protein–protein interactions.<sup>24</sup> The structure described here will help guide the design of small molecule inhibitors of AMA1 with broad strain specificity.

## ■ ASSOCIATED CONTENT

### Supporting Information

<sup>1</sup>H NMR and size-exclusion chromatography of FVO *PfAMA1* (Figure S1), sequence alignment of 3D7 and FVO *PfAMA1* (Figure S2), 3D7 and FVO *PfAMA1* sequence variations in the D1 and D2 polymorphic clusters (Figure S3), crystal packing of the FVO *PfAMA1* Id loop (Figure S4), rmsds of FVO *PfAMA1*, 3D7 *PfAMA1*, and *P. vivax* AMA1 (Figure S5), rmsfs of FVO *PfAMA1*, 3D7 *PfAMA1*, and *P. vivax* AMA1 (Figure S6), crystal packing against the *PfAMA1* DII loop (Figure S7), <sup>1</sup>H–<sup>15</sup>N HSQC spectra of FVO and 3D7 *PfAMA1* (Figure S8), <sup>1</sup>H–<sup>13</sup>C projection of HNCO spectra of FVO and 3D7 *PfAMA1* (Figure S9), SPR of R1–FVO *PfAMA1* interaction (Figure S10), X-ray data collection and refinement statistics (Table S1), average values of normalized B factors for Ia–If and DII loops (Table S2), crystal packing in AMA1 crystal structures (Table S3), FoldX-calculated energies (Table S4), and polar interactions involved in stabilizing the AMA1 Id loops (Table S5). This material is available free of charge via the Internet at <http://pubs.acs.org>.

## ■ AUTHOR INFORMATION

### Corresponding Authors

\*E-mail: ray.norton@monash.edu. Telephone: +613 9903 9167. Fax: +613 9903 9582.

\*E-mail: sheena.mcgowan@monash.edu. Telephone: +613 9902 9309. Fax: +613 9902 9500.

### Funding

S.M. is an Australian Research Council Future Fellow (FT100100690). R.S.N. acknowledges fellowship support from the National Health and Medical Research Council of Australia. This work was supported by the National Health and Medical Research Council (Project Grant 1025150). This research was supported by the Victorian Life Sciences Computation Initiative Life Sciences Computation Centre (RAS Grant VR0316), a collaboration among Melbourne, Monash, and La Trobe Universities and an initiative of the Victorian Government of Australia.

## Notes

The authors declare no competing financial interest.

## ■ ACKNOWLEDGMENTS

We thank Nyssa Drinkwater for technical assistance. We thank the Australian Synchrotron for beam time and technical assistance.

## ■ ABBREVIATIONS

AMA1, apical membrane antigen 1; NMR, nuclear magnetic resonance; HSQC, heteronuclear single-quantum coherence; *Pf*, *P. falciparum*; TROSY, transverse relaxation-optimized spectroscopy; MD, molecular dynamics; SPR, surface plasmon resonance; MWCO, molecular weight cutoff; TEV, tobacco etch virus; LB, Luria broth; IPTG, isopropyl β-D-1-thiogalactopyranoside; rmsd, root-mean-square deviation; rmsf, root-mean-square fluctuation; PEG, polyethylene glycol; MES, 2-(N-morpholino)ethanesulfonic acid; HEPES, 4-(2-hydroxyethyl)-1-piperazineethanesulfonic acid; PME, particle mesh Ewald.

## ■ REFERENCES

- (1) White, N. J., Dondorp, A. M., Faiz, A., Mishra, S., and Hien, T. T. (2012) New global estimates of malaria deaths. *Lancet* 380, 559–560.
- (2) *World Malaria Report* (2013) World Health Organization, Geneva.
- (3) Mendis, K., Sina, B. J., Marchesini, P., and Carter, R. (2001) The neglected burden of *Plasmodium vivax* malaria. *Am. J. Trop. Med. Hyg.* 64, 97–106.
- (4) Duffy, P. E., and Sibley, C. H. (2005) Are we losing artemisinin combination therapy already? *Lancet* 366, 1908–1909.
- (5) Collins, C. R., Withers-Martinez, C., Bentley, G. A., Batchelor, A. H., Thomas, A. W., and Blackman, M. J. (2007) Fine mapping of an epitope recognized by an invasion-inhibitory monoclonal antibody on the malaria vaccine candidate apical membrane antigen 1. *J. Biol. Chem.* 282, 7431–7441.
- (6) Harris, K. S., Casey, J. L., Coley, A. M., Karas, J. A., Sabo, J. K., Tan, Y. Y., Dolezal, O., Norton, R. S., Hughes, A. B., Scanlon, D., and Foley, M. (2009) Rapid optimization of a peptide inhibitor of malaria parasite invasion by comprehensive N-methyl scanning. *J. Biol. Chem.* 284, 9361–9371.
- (7) Henderson, K. A., Streltsov, V. A., Coley, A. M., Dolezal, O., Hudson, P. J., Batchelor, A. H., Gupta, A., Bai, T., Murphy, V. J., Anders, R. F., Foley, M., and Nuttall, S. D. (2007) Structure of an IgNAR-AMA1 complex: Targeting a conserved hydrophobic cleft broadens malarial strain recognition. *Structure* 15, 1452–1466.
- (8) Li, F., Dluzewski, A., Coley, A. M., Thomas, A., Tilley, L., Anders, R. F., and Foley, M. (2002) Phage-displayed peptides bind to the malarial protein apical membrane antigen-1 and inhibit the merozoite invasion of host erythrocytes. *J. Biol. Chem.* 277, 50303–50310.
- (9) Vulliez-Le Normand, B., Tonkin, M. L., Lamarque, M. H., Langer, S., Hoos, S., Roques, M., Saul, F. A., Faber, B. W., Bentley, G. A., Boulanger, M. J., and Lebrun, M. (2012) Structural and functional insights into the malaria parasite moving junction complex. *PLoS Pathog.* 8, e1002755.
- (10) Yap, A., Azevedo, M. F., Gilson, P. R., Weiss, G. E., O'Neill, M. T., Wilson, D. W., Crabb, B. S., and Cowman, A. F. (2014) Conditional expression of apical membrane antigen 1 in *Plasmodium falciparum* shows it is required for erythrocyte invasion by merozoites. *Cell. Microbiol.* 16, 642–656.
- (11) Triglia, T., Healer, J., Caruana, S. R., Hodder, A. N., Anders, R. F., Crabb, B. S., and Cowman, A. F. (2000) Apical membrane antigen 1 plays a central role in erythrocyte invasion by *Plasmodium* species. *Mol. Microbiol.* 38, 706–718.
- (12) Waters, A. P., Thomas, A. W., Deans, J. A., Mitchell, G. H., Hudson, D. E., Miller, L. H., McCutchan, T. F., and Cohen, S. (1990) A merozoite receptor protein from *Plasmodium knowlesi* is highly

- conserved and distributed throughout *Plasmodium*. *J. Biol. Chem.* 265, 17974–17979.
- (13) Hodder, A. N., Crewther, P. E., Matthew, M. L., Reid, G. E., Moritz, R. L., Simpson, R. J., and Anders, R. F. (1996) The disulfide bond structure of *Plasmodium* apical membrane antigen-1. *J. Biol. Chem.* 271, 29446–29452.
- (14) Nair, M., Hinds, M. G., Coley, A. M., Hodder, A. N., Foley, M., Anders, R. F., and Norton, R. S. (2002) Structure of domain III of the blood-stage malaria vaccine candidate, *Plasmodium falciparum* apical membrane antigen 1 (AMA1). *J. Mol. Biol.* 322, 741–753.
- (15) Anders, R. F., Adda, C. G., Foley, M., and Norton, R. S. (2010) Recombinant protein vaccines against the asexual blood stages of *Plasmodium falciparum*. *Hum. Vaccines* 6, 39–53.
- (16) Thera, M. A., Doumbo, O. K., Coulibaly, D., Laurens, M. B., Ouattara, A., Kone, A. K., Guindo, A. B., Traore, K., Traore, I., Kouriba, B., Diallo, D. A., Diarra, I., Daou, M., Dolo, A., Tolo, Y., Sissoko, M. S., Niangaly, A., Sissoko, M., Takala-Harrison, S., Lyke, K. E., Wu, Y., Blackwelder, W. C., Godeaux, O., Vekemans, J., Dubois, M. C., Ballou, W. R., Cohen, J., Thompson, D., Dube, T., Soisson, L., Diggs, C. L., House, B., Lanar, D. E., Dutta, S., Heppner, D. G., Jr., and Plowe, C. V. (2011) A field trial to assess a blood-stage malaria vaccine. *N. Engl. J. Med.* 365, 1004–1013.
- (17) Ouattara, A., Mu, J. B., Takala-Harrison, S., Saye, R., Sagara, I., Dicko, A., Niangaly, A., Duan, J. H., Ellis, R. D., Miller, L. H., Su, X. Z., Plowe, C. V., and Doumbo, O. K. (2010) Lack of allele-specific efficacy of a bivalent AMA1 malaria vaccine. *Malar. J.* 9, 175.
- (18) Dutta, S., Slugosz, L. S., Drew, D. R., Ge, X., Ababacar, D., Rovira, Y. I., Moch, J. K., Shi, M., Long, C. A., Foley, M., Beeson, J. G., Anders, R. F., Miura, K., Haynes, J. D., and Batchelor, A. H. (2013) Overcoming antigenic diversity by enhancing the immunogenicity of conserved epitopes on the malaria vaccine candidate apical membrane antigen-1. *PLoS Pathog.* 9, e1003840.
- (19) Miura, K., Herrera, R., Diouf, A., Zhou, H., Mu, J., Hu, Z., MacDonald, N. J., Reiter, K., Nguyen, V., Shimp, R. L., Jr., Singh, K., Narum, D. L., Long, C. A., and Miller, L. H. (2013) Overcoming allelic specificity by immunization with five allelic forms of *Plasmodium falciparum* apical membrane antigen 1. *Infect. Immun.* 81, 1491–1501.
- (20) Dutta, S., Lee, S. Y., Batchelor, A. H., and Lanar, D. E. (2007) Structural basis of antigenic escape of a malaria vaccine candidate. *Proc. Natl. Acad. Sci. U.S.A.* 104, 12488–12493.
- (21) Harris, K. S., Adda, C. G., Khore, M., Drew, D. R., Valentini-Gatt, A., Fowkes, F. J., Beeson, J. G., Dutta, S., Anders, R. F., and Foley, M. (2014) Immunodampening to overcome diversity in the malarial vaccine candidate apical membrane antigen 1. *Infect. Immun.* DOI: 10.1128/IAI.02061-14.
- (22) Tonkin, M. L., Crawford, J., Lebrun, M. L., and Boulanger, M. J. (2013) *Babesia divergens* and *Neospora caninum* apical membrane antigen 1 structures reveal selectivity and plasticity in apicomplexan parasite host cell invasion. *Protein Sci.* 22, 114–127.
- (23) Bai, T., Becker, M., Gupta, A., Strike, P., Murphy, V. J., Anders, R. F., and Batchelor, A. H. (2005) Structure of AMA1 from *Plasmodium falciparum* reveals a clustering of polymorphisms that surround a conserved hydrophobic pocket. *Proc. Natl. Acad. Sci. U.S.A.* 102, 12736–12741.
- (24) Lim, S. S., Debono, C. O., MacRaile, C. A., Chandrashekaran, I. R., Dolezal, O., Anders, R. F., Simpson, J. S., Scanlon, M. J., Devine, S. M., Scammells, P. J., and Norton, R. S. (2013) Development of inhibitors of *Plasmodium falciparum* apical membrane antigen 1 based on fragment screening. *Aust. J. Chem.* 66, 1530–1536.
- (25) MacRaile, C. A., Anders, R. F., Foley, M., and Norton, R. S. (2011) Apical membrane antigen 1 as an anti-malarial drug target. *Curr. Top. Med. Chem.* 11, 2039–2047.
- (26) Srinivasan, P., Yasgar, A., Luci, D. K., Beatty, W. L., Hu, X., Andersen, J., Narum, D. L., Moch, J. K., Sun, H., Haynes, J. D., Maloney, D. J., Jadhav, A., Simeonov, A., and Miller, L. H. (2013) Disrupting malaria parasite AMA1–RON2 interaction with a small molecule prevents erythrocyte invasion. *Nat. Commun.* 4, 2261.
- (27) Coley, A. M., Gupta, A., Murphy, V. J., Bai, T., Kim, H., Foley, M., Anders, R. F., and Batchelor, A. H. (2007) Structure of the malaria antigen AMA1 in complex with a growth-inhibitory antibody. *PLoS Pathog.* 3, 1308–1319.
- (28) Coley, A. M., Parisi, K., Masciantonio, R., Hoeck, J., Casey, J. L., Murphy, V. J., Harris, K. S., Batchelor, A. H., Anders, R. F., and Foley, M. (2006) The most polymorphic residue on *Plasmodium falciparum* apical membrane antigen 1 determines binding of an invasion-inhibitory antibody. *Infect. Immun.* 74, 2628–2636.
- (29) Harris, K. S., Casey, J. L., Coley, A. M., Masciantonio, R., Sabo, J. K., Keizer, D. W., Lee, E. F., McMahon, A., Norton, R. S., Anders, R. F., and Foley, M. (2005) Binding hot spot for invasion inhibitory molecules on *Plasmodium falciparum* apical membrane antigen 1. *Infect. Immun.* 73, 6981–6989.
- (30) Sivashanmugam, A., Murray, V., Cui, C., Zhang, Y., Wang, J., and Li, Q. (2009) Practical protocols for production of very high yields of recombinant proteins using *Escherichia coli*. *Protein Sci.* 18, 936–948.
- (31) Salzmann, M., Pervushin, K., Wider, G., Senn, H., and Wuthrich, K. (1998) TROSY in triple-resonance experiments: New perspectives for sequential NMR assignment of large proteins. *Proc. Natl. Acad. Sci. U.S.A.* 95, 13585–13590.
- (32) Riek, R., Pervushin, K., and Wüthrich, K. (2000) TROSY and CRINEPT: NMR with large molecular and supramolecular structures in solution. *Trends Biochem. Sci.* 25, 462–468.
- (33) Chesne-Seck, M. L., Pizarro, J. C., Vulliez-Le Normand, B., Collins, C. R., Blackman, M. J., Faber, B. W., Remarque, E. J., Kocken, C. H., Thomas, A. W., and Bentley, G. A. (2005) Structural comparison of apical membrane antigen 1 orthologues and paralogues in apicomplexan parasites. *Mol. Biochem. Parasitol.* 144, 55–67.
- (34) Gunasekera, A. M., Wickramaratne, T., Neafsey, D. E., Ganguli, I., Perera, L., Premaratne, P. H., Hartl, D., Handunnetti, S. M., Udagama-Randeniya, P. V., and Wirth, D. F. (2007) Genetic diversity and selection at the *Plasmodium vivax* apical membrane antigen-1 (*PvAMA-1*) locus in a Sri Lankan population. *Mol. Biol. Evol.* 24, 939–947.
- (35) Remarque, E. J., Faber, B. W., Kocken, C. H., and Thomas, A. W. (2008) Apical membrane antigen 1: A malaria vaccine candidate in review. *Trends Parasitol.* 24, 74–84.
- (36) Kabsch, W. (2010) Xds. *Acta Crystallogr. D66*, 125–132.
- (37) Evans, P. R., and Murshudov, G. N. (2013) How good are my data and what is the resolution? *Acta Crystallogr. D69*, 1204–1214.
- (38) Collaborative Computational Project, No. 4 (1994) The CCP4 suite: Programs for protein crystallography. *Acta Crystallogr. D50*, 760–763.
- (39) Brunger, A. T. (1993) Assessment of phase accuracy by cross validation: The free *R* value. Methods and applications. *Acta Crystallogr. D49*, 24–36.
- (40) McCoy, A. J., Grosse-Kunstleve, R. W., Storoni, L. C., and Read, R. J. (2005) Likelihood-enhanced fast translation functions. *Acta Crystallogr. D61*, 458–464.
- (41) Adams, P. D., Afonine, P. V., Bunkóczki, G., Chen, V. B., Davis, I. W., Echols, N., Headd, J. J., Hung, L.-W., Kapral, G. J., Grosse-Kunstleve, R. W., McCoy, A. J., Moriarty, N. W., Oeffner, R., Read, R. J., Richardson, D. C., Richardson, J. S., Terwilliger, T. C., and Zwart, P. H. (2010) PHENIX: A comprehensive Python-based system for macromolecular structure solution. *Acta Crystallogr. D66*, 213–221.
- (42) Afonine, P. V., Grosse-Kunstleve, R. W., Echols, N., Headd, J. J., Moriarty, N. W., Mustyakimov, M., Terwilliger, T. C., Urzhumtsev, A., Zwart, P. H., and Adams, P. D. (2012) Towards automated crystallographic structure refinement with phenix.refine. *Acta Crystallogr. D68*, 352–367.
- (43) Emsley, P., and Cowtan, K. (2004) Coot: Model-building tools for molecular graphics. *Acta Crystallogr. D60*, 2126–2132.
- (44) Krissinel, E., and Henrick, K. (2007) Inference of macromolecular assemblies from crystalline state. *J. Mol. Biol.* 372, 774–797.
- (45) Androulakis, S., Schmidberger, J., Bate, M. A., DeGori, R., Beitz, A., Keong, C., Cameron, B., McGowan, S., Porter, C. J., Harrison, A., Hunter, J., Martin, J. L., Kobe, B., Dobson, R. C., Parker, M. W., Whisstock, J. C., Gray, J., Treloar, A., Groenewegen, D., Dickson, N.,

- and Buckle, A. M. (2008) Federated repositories of X-ray diffraction images. *Acta Crystallogr. D* 64, 810–814.
- (46) Tronrud, D. E. (1996) Knowledge-based B-factor restraints for the refinement of proteins. *J. Appl. Crystallogr.* 29, 100–104.
- (47) Parthasarathy, S., and Murthy, M. R. N. (1997) Analysis of temperature factor distribution in high-resolution protein structures. *Protein Sci.* 6, 2561–2567.
- (48) Molecular Operating Environment (MOE) (2012) CCGI, Montreal, QC.
- (49) Jorgensen, W. L., Chandrasekhar, J., Madura, J. D., Impey, R. W., and Klein, M. L. (1983) Comparison of simple potential functions for simulating liquid water. *J. Chem. Phys.* 79, 926–935.
- (50) Phillips, J. C., Braun, R., Wang, W., Gumbart, J., Tajkhorshid, E., Villa, E., Chipot, C., Skeel, R. D., Kale, L., and Schulten, K. (2005) Scalable molecular dynamics with NAMD. *J. Comput. Chem.* 26, 1781–1802.
- (51) Case, D., Darden, T., Cheatham, T., III, Simmerling, C., Wang, J., Duke, R., Luo, R., Walker, R., Zhang, W., and Merz, K. (2012) AMBER 12, University of California, San Francisco.
- (52) Hornak, V., Abel, R., Okur, A., Strockbine, B., Roitberg, A., and Simmerling, C. (2006) Comparison of multiple Amber force fields and development of improved protein backbone parameters. *Proteins: Struct., Funct., Bioinf.* 65, 712–725.
- (53) Wickstrom, L., Okur, A., and Simmerling, C. (2009) Evaluating the performance of the ff99SB force field based on NMR scalar coupling data. *Biophys. J.* 97, 853–856.
- (54) Essmann, U., Perera, L., Berkowitz, M. L., Darden, T., Lee, H., and Pedersen, L. G. (1995) A smooth particle mesh Ewald method. *J. Chem. Phys.* 103, 8577–8593.
- (55) Hess, B., Kutzner, C., van der Spoel, D., and Lindahl, E. (2008) GROMACS 4: Algorithms for highly efficient, load-balanced, and scalable molecular simulation. *J. Chem. Theory Comput.* 4, 435–447.
- (56) Humphrey, W., Dalke, A., and Schulten, K. (1996) VMD: Visual molecular dynamics. *J. Mol. Graphics* 14, 33–38.
- (57) Baker, N. A., Sept, D., Joseph, S., Holst, M. J., and McCammon, J. A. (2001) Electrostatics of nanosystems: Application to microtubules and the ribosome. *Proc. Natl. Acad. Sci. U.S.A.* 98, 10037–10041.
- (58) Schymkowitz, J., Borg, J., Stricher, F., Nys, R., Rousseau, F., and Serrano, L. (2005) The FoldX web server: An online force field. *Nucleic Acids Res.* 33, W382–W388.
- (59) Pizarro, J. C., Vulliez-Le Normand, B., Chesne-Seck, M. L., Collins, C. R., Withers-Martinez, C., Hackett, F., Blackman, M. J., Faber, B. W., Remarque, E. J., Kocken, C. H., Thomas, A. W., and Bentley, G. A. (2005) Crystal structure of the malaria vaccine candidate apical membrane antigen 1. *Science* 308, 408–411.
- (60) Ge, X., MacRaild, C. A., Devine, S. M., Debono, C. O., Wang, G., Scammells, P. J., Scanlon, M. J., Anders, R. F., Foley, M., and Norton, R. S. (2014) Ligand-induced conformational change of *Plasmodium falciparum* AMA1 detected using <sup>19</sup>F NMR. *J. Med. Chem.* 57, 6419–6427.
- (61) Guerois, R., Nielsen, J. E., and Serrano, L. (2002) Predicting changes in the stability of proteins and protein complexes: A study of more than 1000 mutations. *J. Mol. Biol.* 320, 369–387.
- (62) Schymkowitz, J. W. H., Rousseau, F., Martins, I. C., Ferkinghoff-Borg, J., Stricher, F., and Serrano, L. (2005) Prediction of water and metal binding sites and their affinities by using the Fold-X force field. *Proc. Natl. Acad. Sci. U.S.A.* 102, 10147–10152.
- (63) Hehl, A. B., Lekutis, C., Grigg, M. E., Bradley, P. J., Dubremetz, J. F., Ortega-Barria, E., and Boothroyd, J. C. (2000) *Toxoplasma gondii* homologue of *Plasmodium* apical membrane antigen 1 is involved in invasion of host cells. *Infect. Immun.* 68, 7078–7086.
- (64) Lamarque, M., Besteiro, S., Papoin, J., Roques, M., Vulliez-Le Normand, B., Morlon-Guyot, J., Dubremetz, J. F., Fauquenoy, S., Tomavo, S., Faber, B. W., Kocken, C. H., Thomas, A. W., Boulanger, M. J., Bentley, G. A., and Lebrun, M. (2011) The RON2-AMA1 interaction is a critical step in moving junction-dependent invasion by apicomplexan parasites. *PLoS Pathog.* 7, e1001276.
- (65) Takala, S. L., Coulibaly, D., Thera, M. A., Batchelor, A. H., Cummings, M. P., Escalante, A. A., Ouattara, A., Traore, K., Niangaly, A., Djimde, A. A., Doumbo, O. K., and Plowe, C. V. (2009) Extreme polymorphism in a vaccine antigen and risk of clinical malaria: Implications for vaccine development. *Sci. Transl. Med.* 1, 2ra5.
- (66) Ouattara, A., Takala-Harrison, S., Thera, M. A., Coulibaly, D., Niangaly, A., Saye, R., Tolo, Y., Dutta, S., Heppner, D. G., Soisson, L., Diggs, C. L., Vekemans, J., Cohen, J., Blackwelder, W. C., Dube, T., Laurens, M. B., Doumbo, O. K., and Plowe, C. V. (2013) Molecular basis of allele-specific efficacy of a blood-stage malaria vaccine: Vaccine development implications. *J. Infect. Dis.* 207, 511–519.